FINAL TECHNICAL REPORT

Project Title: IMPLICATIONS OF GRAPHITE RADIATION DAMAGE ON THE NEUTRONIC, OPERATIONAL, AND SAFETY ASPECTS OF VERY HIGH TEMPERATURE REACTORS

Covering Period: July 1st, 2007 through May 31st, 2011

Date of Report: August 30, 2011

Recipient:
North Carolina Sate University
P.O. Box 7909
Department of Nuclear Engineering
Raleigh, NC 27695-7909

Award Number: DE-FC07-07ID14818 (NERI 07-011)

Subcontractors: N/A

Other Partners: Oak Ridge National Laboratory

Idaho National Laboratory

Contact(s):
Ayman I. Hawari
(919) 515-4598
ayman.hawari@ncsu.edu

Project Objective: In both the prismatic and pebble bed designs of Very High Temperature Reactors (VHTR), the graphite moderator is expected to reach exposure levels of 10^{21} to 10^{22} n/cm^2 over the lifetime of the reactor. This exposure results in damage to the graphite structure. In this work, molecular dynamic and ab initio molecular static calculations will be used to: 1) simulate radiation damage in graphite under various irradiation and temperature conditions, 2) generate the thermal neutron scattering cross sections for damaged graphite, and 3) examine the resulting microstructure to identify damage formations that may produce the high-temperature Wigner effect. The impact of damage on the neutronic, operational and safety behavior of the reactor will be assessed using reactor physics calculations. In addition, tests will be performed on irradiated graphite samples to search for the high-temperature Wigner effect, and phonon density of states measurements will be conducted to quantify the effect on thermal neutron scattering cross sections using these samples.

Background: Generation IV Very High Temperature Reactor (VHTR) concepts, which are currently under study as power and hydrogen production units, are based on graphite moderated and gas cooled nuclear reactors. Upon exposure to the doses of neutron radiation expected in a VHTR (10^{21} to 10^{22} n/cm^2), graphite will suffer from substantial damage to its microstructure. On the microscopic scale, this damage consists of the formation of Frenkel pairs (i.e., vacancies and interstitials) that can migrate and cluster. Macroscopically, the damage manifests itself in increasing the stored (i.e., Wigner or Wigner-like) energy of the crystal, and in changes in the mechanical, thermal, and electrical properties of the material, as well as in directional dimensional changes. In the past, such effects have been studied and well documented. However, two major observations stand out regarding the current understanding of the phenomenon of radiation damage in graphite: 1) to date, no work exists on the effect of radiation on the neutronic behavior (i.e., thermal neutron scattering properties) of graphite, and 2) evidence for the existence of stable damage formations at high temperatures (T > 1200 °C) and the potential of a high-temperature Wigner-like energy release are recognized but generally underplayed. Clearly, both of these observations can have significant implications on the neutronic, operational, and safety aspects of VHTRs.

Summary: This project represents a unique connection between the worlds of nuclear reactor physics/analysis and reactor materials for the development of the VHTR. During the project, atomistic simulation techniques, based on classical molecular dynamics (MD), were developed to investigate the phenomenon of radiation damage in graphite and to examine the impact on the dynamic structure factor. Furthermore, calculations were performed to estimate the thermal neutron scattering cross sections of graphite for both unirradiated and irradiated structures. To assure the accuracy of such calculations, methods were developed to correct the classical MD results to account for quantum mechanical effects such as detailed balance and atomic recoil. The developed correction approach is shown to be universal and should apply to various crystalline materials. In addition, the MD simulations were also used to explore the concept of stored energy in irradiated graphite and to predict its magnitude as damage cascades are initiated in a modeled graphite supercell. Experimentally, the investigation involved performing neutron scattering studies on graphite. Powder diffraction measurements were conducted and tools were developed to analyze the powder diffraction patterns of both unirradiated and irradiated graphite samples. Positron annihilation lifetime spectrometry was also performed to understand the porosity structure in graphite, which confirmed a significant increase in the nanoporosity concentration in irradiated graphite.

1. Molecular Dynamics Models and Thermal Scattering in Graphite

The computational effort for this project was initiated using the NCSU graphite molecular dynamics (MD) tools that have been developed over the past few years. The methodology developed was validated for temperatures extending from a few degrees K to around 2000 K, which includes temperatures relevant for the VHTR. In the current work, the MD methodology was extended to enable calculating and extracting all the quantities that are relevant in thermal neutron scattering studies. One connection between molecular dynamics and thermal neutron scattering lies in the dynamic pair correlation function, $G(\vec{r},t)$, which represents the probability of finding an atom at position $\vec{r}$ at time t. Under the Van Hove formulation, the Fourier transform of $G(\vec{r},t)$ in space and time is equal to the scattering law of the material

$$S(\vec{Q},w)=\frac{1}{2\pi\hbar}\int_{-\infty}^{\infty}\int_{-\infty}^{\infty}G(\vec{r},t)e^{i(\vec{Q}\cdot\vec{r}-wt)}d\vec{r}dt\,,$$

where $\vec{Q}=\vec{k}-\vec{k}'$, k and k' represent the magnitude of the wave vector of the incident and scattered neutron respectively, $\hbar$ is the reduced Planck constant, and ω is the vibrational frequency. The scattering law may be decomposed into two terms

$$S(\vec{Q},w)=S_s(\vec{Q},w)+S_d(\vec{Q},w)$$

where S_s is the self scattering law and S_d is the distinct scattering law. The former is associated with the autocorrelation of each atom's position, whereas the latter involves the correlation between the positions of different atoms. Given the scattering law, the differential scattering cross section may be calculated as

$$\frac{d^2\sigma}{d\Omega dE}=\frac{1}{4\pi}\frac{k'}{k}\left(\sigma_{coh}S(\vec{Q},w)+\sigma_{incoh}S_s(\vec{Q},w)\right),$$

where σ_{coh} is the bound atom coherent scattering cross section and σ_{incoh} is the bound atom incoherent scattering cross section.

The advantage of the Van Hove approach described above is that it applies to both damaged and undamaged systems and includes all temperature anharmonic effects.

2. Thermal Neutron Scattering Cross Sections

The total inelastic scattering law of graphite (distinct + self) has been evaluated from MD correlation functions at 300 K and 533 K and compared against measured data. The computational effort of the $S_d(\alpha,\beta)$ calculation was reduced considerably by invoking the coherent Gaussian approximation beyond a certain cutoff radius, which is justifiable in the case that correlated motion is negligible beyond that distance. This is generally a good approximation outside of the close neighbor shells. The intermediate function is therefore calculated as

$$I_{j,j'}(\kappa,t) = \begin{cases} \left\langle \exp\left(-i\vec{\kappa}\cdot\vec{r}_j(0)\right)\cdot\exp\left(i\vec{\kappa}\cdot\vec{r}_{j'}(t)\right)\right\rangle & if \quad R < R_{cut} \\ \exp\left[\frac{-\kappa^2}{6}\left\langle\left(r_j(t)-r_{j'}(0)\right)^2\right\rangle\right] & if \quad R > R_{cut} \end{cases}$$

where $R = \left|\vec{r}_j - \vec{r}_{j'}\right|$ and, in the present work, the summation over *j* runs over the centermost 20 atoms of the system, while the *j'* index runs over all 9600 atoms comprising the supercell. An R_{cut} value of 3.7Å was selected in order to ensure that correlations in the first few coordination shells were evaluated exactly.

Limited experimental data for $S(\alpha,\beta)$ at 300 K is available and is plotted alongside the total $S(\alpha,\beta)$ from MD in Fig. 1. An excellent benchmark of the MD coherent calculation is the set of experimental scattering law data published by Carvalho for 533 K graphite. Carvalho's data, complete with uncertainty estimates, shows clearly the oscillations that $S_d(\alpha,\beta)$ superimposes onto the normally smooth $S_s(\alpha,\beta)$. Comparisons are also drawn against the exact $S_s(\alpha,\beta)$ + 1-phonon $S_d(\alpha,\beta)$ curves developed in prior *ab-initio* work]. Figures 1 and 2 demonstrate that oscillations in the MD $S(\alpha,\beta)$ are in-phase with those of the 1-phonon distinct calculation, and, furthermore, that the MD scattering law exhibits similarly good agreement with experimental measurements.

To study the effects of amorphization, a 4,000 atom graphite supercell was heated to 9000 K (far beyond the melting temperature) and then quenched at a rate of 2000 K per 2.5 picoseconds to a final temperature of 300 K. Densities of 1.7 g/cm^3 and 2.23 g/cm^3 were selected for investigation. The relative proportions of sp, sp^2, and sp^3 bonded atoms in the amorphous structure are given in Table 1, and associated phonon frequency distributions are plotted in Fig. 3. Comparisons are drawn to a set of neutron spectroscopy measurements of $\rho(\omega)$ performed on sputtered and glassy carbon samples. A particularly close

correspondence is observed between the MD ρ(ω) and the glassy carbon sample, which is not surprising, since the proportion of sp^3 binding is extremely small in both cases.

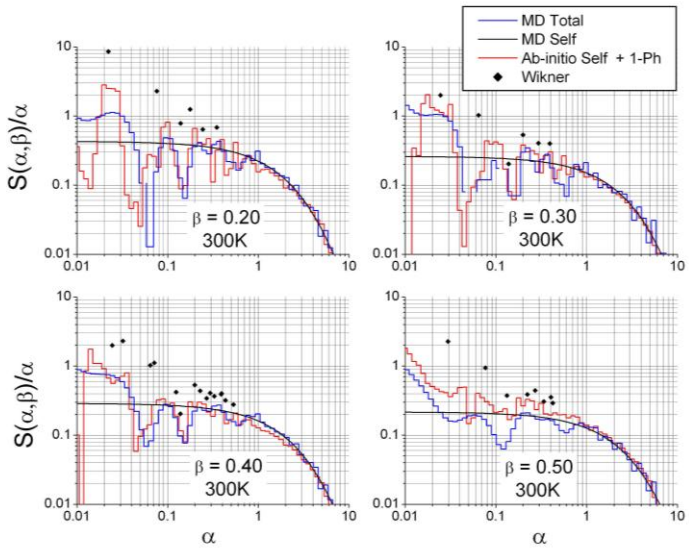

Fig. 1. Total scattering law of graphite at 300 K, including coherent effects.

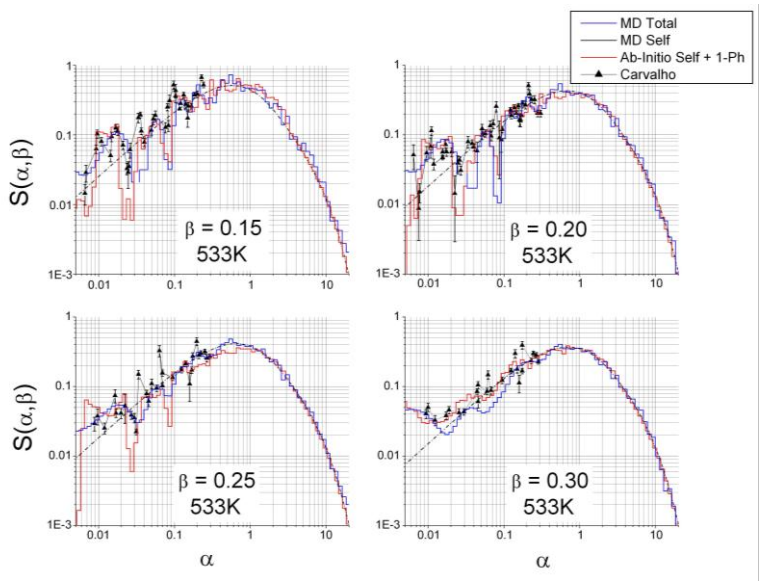

Fig. 2. Total scattering law of graphite at 533 K, including coherent effects.

Table 1. Relative proportions of sp, sp^2, and sp^3 bonded atoms in the amorphous MD structure.

	1.7 g/cm^3	2.23 g/cm^3
sp	0.20	0.07
sp^2	0.79	0.92
sp^3	0.01	0.02

Radiation damage was introduced to an 8000-atom MD supercell through a series of 1.5 keV cascades that were initiated from random lattice sites and always directed towards the center of the system. Cross section analysis was performed only on the damaged region of the supercell, herein defined as all atoms that possessed (at any point in the simulation) a kinetic energy in excess of the threshold displacement energy (E_d) of graphite, as well as all neighbors of those atoms.

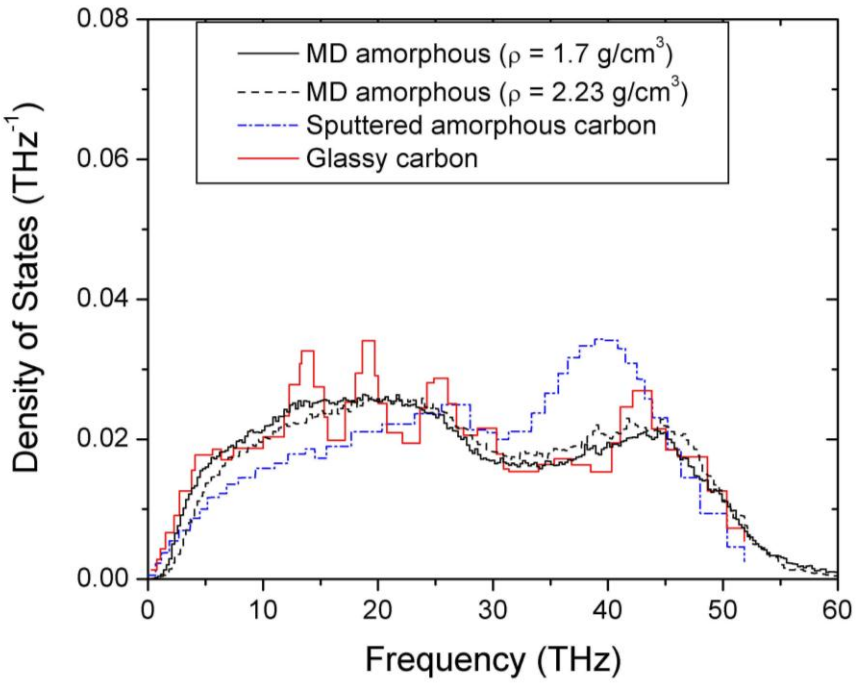

Fig. 3. MD ρ(ω) versus the measured distributions of sputtered and glassy carbon.

Figure 4 shows the cross section effect of sequential cascades in the graphite system. The displayed set of plots includes a snapshot of the atoms comprising the damaged region of the supercell; from the time-dependent positions of these atoms, the incoherent cross section of the damaged region was determined by employing the correlation function

methods developed in earlier work. Also shown is the damage effect on ρ(β). According to this analysis, cascade-induced damage raises the cross section by as much as 48%, with the most sizable difference observed in the incident energy range of 0.01 – 0.03 eV.

As the level of damage increases, and especially at high frequencies, ρ(β) shows an unmistakable evolution towards the frequency distribution of amorphous carbon. Noteworthy similarities include the enhanced availability of vibrational modes in the range of β =1 to β = 2, as well as the shallowing and shifting of the trough at β = 2.75. The sharp peak in the MD distribution just above 50 THz is conspicuously dampened by cascade damage buildup, which is to be expected since the concentration of damage is gradually transforming the system into a more isotropic state, thereby breaking the 2D honeycomb arrangement that is responsible for the high-energy optical modes.

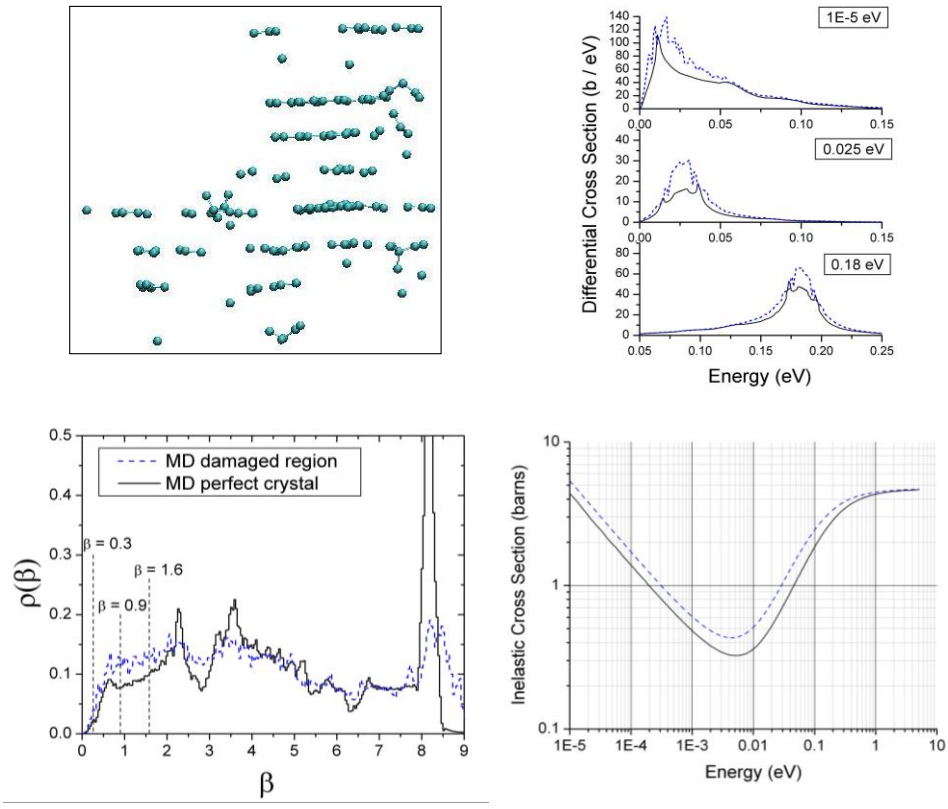

Fig. 4. Damage effect on ρ(β) and the total and differential cross sections following (1) 1.5 keV cascades initiated at 300 K.

3. Stored Energy

Recognized by E.P. Wigner and investigated by later workers the issue of the buildup and release of stored energy has long been a concern in graphite-moderated reactors due to the possibility of a runaway temperature transient. While the stored energy is measurable indirectly using calorimetry, it is quite accessible computationally because the potential energy is a fundamental output variable of MD (or *ab-initio*). The quantity of interest is the average change in potential energy (per atom) brought about by defect accumulation, conventionally converted to units such as J/g.

Figure 5 shows the change in the average potential energy of an 8000 atom supercell as randomly-located 1.5 keV cascades are initiated in the system. Each cascade causes a spike in the potential energy that is partially dissipated by recombination processes, with the end result that the system settles out in a quasi-stable, higher-energy state. The system is only quasi-stable because, over long periods of time (relative to the standard timescale of MD), diffusional processes will instigate further defect recombination, and the system gradually transitions to a lower-energy state. For the purposes of MD, quasi-stability is usually achieved shortly after the cascade-induced temperature spike had dissipated. From Fig. 5, the thermal spike is observed to quench within a few picoseconds of the cascade event.

In a closed supercell, stored energy does not accumulate linearly with respect to the introduced cascade energy; this is a consequence of the interaction of the cascading atoms with the products of previous cascades. Simply stated, less energy will be stored in a region that is already damaged. This effect, which has been confirmed by experimental studies, is apparent in the MD results of Fig. 5 where the incremental change in potential energy decreases (on average) in the later cascades.

The total stored energy is given by the formula:

$$E_s = N\left(E_p - E_p^0\right)$$

Where E_p is the final potential energy (per atom), E_p^0 is the initial potential energy and *N* is the number of atoms in the supercell. For the MD simulation of 15 1.5 keV cascades (Fig. 5), E_s was calculated to be 2.68 keV, which is about 12% of the total cascade energy. The remaining 88% represents kinetic energy that was removed by the thermal bath. On an intrinsic basis, this corresponds to a stored energy of 2740 J/g (655

cal/g), which accords well with the value of 600 cal/g cited in the literature as an upper bound in heavily irradiated graphite.

Figure 6 shows a representation of the MD simulated damage in the graphite structure due to the random introduction of the displacement cascades.

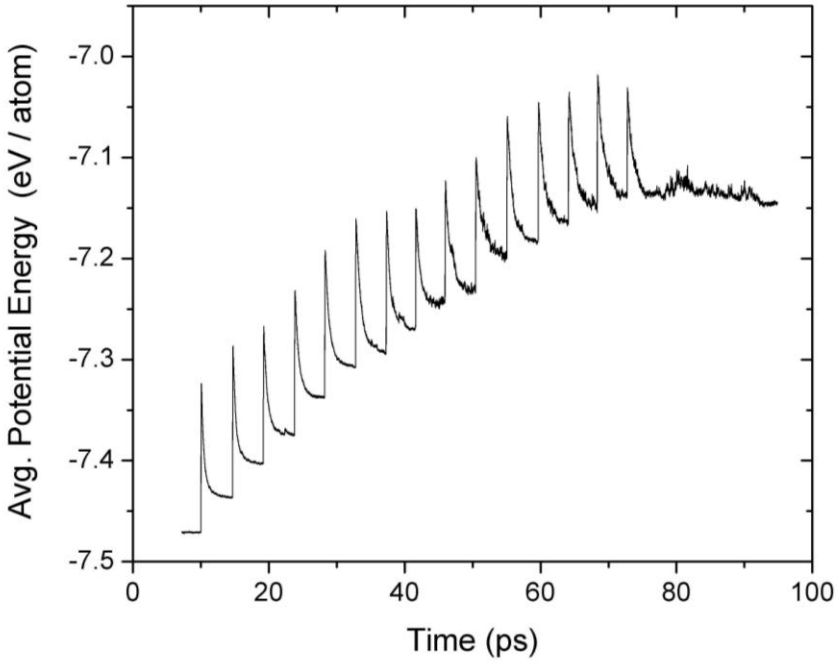

Fig. 5. Buildup of stored energy in a 300K MD graphite supercell. Each spike represents a 1.5 keV cascade event.

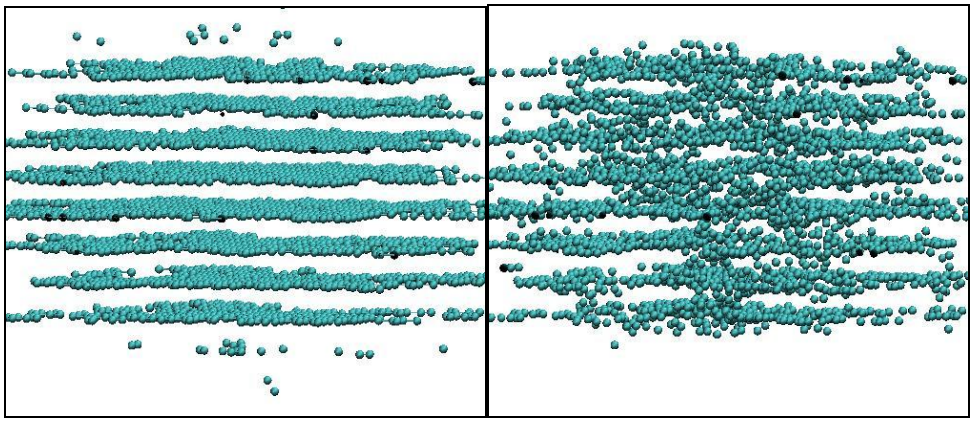

Fig. 6. A representative MD model of the graphite system before the introduction of the cascades (left) and after damage (right).

4. Experimental Measurements

Experimentally, grade NBG-10 unirradiated and irradiated graphite samples were received from ORNL. The irradiated samples include short sections of bend bars numbers L03115-L25 (4.9 x 10^{25} n/m^2 [E>0.1 MeV] at ~280C) and L3124-L69 (4.7 x 10^{25} n/m^2 [E>0.1 MeV] at ~700C). A picture of these samples is shown Fig. 7 below. These samples are used in various measurements that aim at understanding the structure and dynamics of graphite. This includes neutron powder diffraction measurements, neutron inelastic scattering measurements, and positron annihilation measurements.

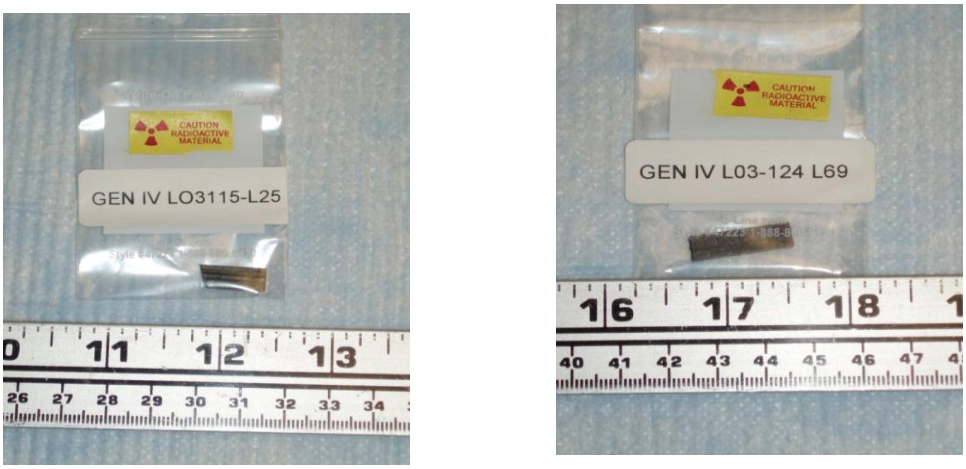

Fig. 7. irradiated graphite samples as received from ORNL.

Neutron Powder Diffraction

Neutron diffraction measurements were carried out at the PULSTAR Neutron Powder Diffractometer using three reactor grade graphite samples. Their dimension, weight, fast neutron exposure dose, and the irradiation temperatures are listed in Table 2. The samples were placed inside a vanadium sample holder and mounted at the sample position. No Bragg peaks are expected to result from the holder since the coherent scattering length of vanadium is very small.

Table 2. The dimension, weight, fast neutron dose, and temperature of the three samples.

Specimen	Dimension (inch)	Weight (g)	Dose (n/m^2)	T (°C)
SGL-NBG-10-S2	1.9x0.255x0.155	1.97	n/a	n/a
GEN IV L03-124-L69	0.9x0.268x0.115	0.70	4.7x10^{25}	700
GEN IV L03-115-L25	0.608x0.267x0.117	0.47	4.9x10^{25}	280

Two models of the graphite structure were assumed. The first is the two-layer model and the second is the one-layer model. The basic unit of the two-layer model is a two AB registered stacking layers package with finite lateral extent. The d-spacing between the two layers is d_{002} without fluctuation. The three stacking options are as follows (see Figure 8):

1) A random shift between the adjacent packages with probability P. The two packages have no phase correlation (Figure 8a).
2) A registered shift between the adjacent packages with probability P_t. The A layer in the package above move to the C stacking reference to the A layer in the package below, and the B layer in the package above will move to the A stacking reference to the A layer in the package below. Local ABC stacking appears (Figure 8b).
3) No shift at all with probability (1-P-P_t), which gives local ABAB stacking (Figure 8c).

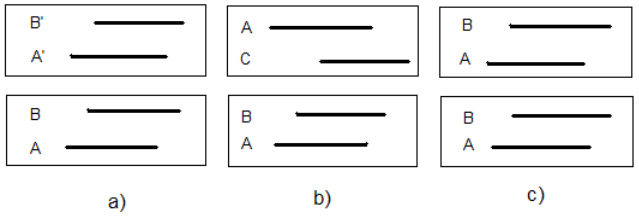

Fig. 8. The three possible stacking of two adjacent packages. The bold line represents the basal layer.

Clearly, this model can simulate the ABAB stacking, the ABCABC stacking, and graphite with some ABC and/or random shift stacking faults. But it cannot model the structure with the probability of stacking fault above 0.5, since half the neighboring layers are constrained with AB stacking.

A parameter δ, where $<\delta>=0$, and $<\delta^2>\neq 0$, was introduced to model the d-spacing fluctuation. It is assumed that the d-spacing fluctuation is only happening between the two packages. The probability of a given fluctuation δ follows the Gaussian distribution:

$$p(\delta) = \frac{1}{\sqrt{2\pi\left\langle \delta^2 \right\rangle}} e^{-\delta^2/(2<\delta^2>)}$$

In the one-layer model, the basic unit is a carbon layer with honeycomb arrangement, which is then stacked to form the structure. If a particular layer is said to occupy the A position, then the next layer can be:

1) a random shift layer with probability P;
2) a layer occupied the B position with probability (1-P)/2;
3) a layer occupied the C position with probability (1-P)/2.

This model cannot reproduce the ABAB and ABCABC stacking found in crystalline graphite, but it can describe the most disordered carbon adequately. For totally turbostratic disordered carbon, the probability of random shift layer should be 1.0.

A combination of a Dirac delta function and a Gaussian distribution is given to describe the d-spacing fluctuation. The formula is given as

$$P(\delta) = g\delta_D(\delta) + (1-g)\frac{1}{\sqrt{2\pi < \delta^2 >}} e^{-\delta^2/(2<\delta^2>)}$$

In the first term of the above equation, g is a number between zero and one, which represents the fraction of low-strain portion in graphite. In the second term, the Gaussian distribution represents the portion in graphite with d-spacing fluctuation.

There are other parameters of this model, such as the in-plane lattice constant, number of the basic unit in the two models, lateral size of the crystallite, the preferential orientation, the isotropic temperature factor, and the in-plane strain parameter. All these parameters are listed in Table 3.

A non-linear least squares method is applied to minimize the residual between the observed and calculated intensity. The residual S is defined as following

$$S = \sum_i \omega_i (y_i - y_{ci})^2 ,$$

where i is the step number, y_i is the observed intensity at ith step, y_{ci} is the calculated intensity at the ith step, and ω_i is the weight factor at ith step. It is $1/y_i$. The goodness of fit (χ^2) is defined as:

$$\chi^2 = \frac{S}{N-P},$$

where N is the total number of steps, and P is the number of refined parameters.

Table 3. parameters used in the two-layer package model and one-layer model

Parameters	Two-layer model	One-layer model
Inter planar spacing	d_{002}	d_{002}
In-plane lattice constant	a	A
Probability of random shift between adjacent unit	P	P
Probability of 3R stacking between two adjacent unit	P_t	
Fraction of unorganized carbon		(1-g)
In-plane strain parameter		Z
Fluctuation of d spacing between adjacent two layers	$\frac{1}{2}\sqrt{<\delta^2>}$	$\sqrt{<\delta>^2}$
Number of stacking units in the crystallite	M	M
Lateral size of the crystallite	L_a	L_a
Preferred orientation	P_0	P_0
Isotropic temperature factor	B	B

The un-irradiated sample and the one irradiated at temperature 700°C are materials with graphite structure. Their neutron diffraction patterns can be fitted by the two-layer model mentioned above and are shown in Figure 9a and 9b, and the refined parameters are given in Table 4. The parameters in Table 4 can be classified as axial stacking parameters: d_{002}, $<\delta^2>^{1/2}$, M, P, and P_t; the plane structure parameters: a, and L_a; the atom thermal motion parameter B, and the preferred orientation parameter p_0 of the sample. According to Table 4, we can find that the irradiation damage reduces the probabilities of ordered AB and ABC stacking, the number of the packages stacked in one crystallite, the lattice parameter a, the lateral dimension; and increases the probability of random stacking, the isotropic temperature factor, and the inter-layer d spacing and its fluctuation.

The displaced carbon atoms favor going to the interlayer space due to the relatively large interlayer space. The interstitial atoms can move and form interstitial loops, and these loops will increase the interlayer d spacing locally, and increase the average interlayer d spacing and its fluctuation. At the same time, the existence of the interstitial atoms and loops will force their neighbor layers to shift randomly so the probability of random shifting is increased.

The vacancy defects in the crystal lattice can distort the lattice in the plane locally, and this distortion will cause the contraction along the a axis and the entire lateral dimension. The vacancy defects in the crystal lattice may join together to form vacancy loops which may collapse the basal planes, and the total number of two-plane packages in the crystallite is reduced. The existence of vacancy defects affects the environment of their neighbor carbon atoms, and the isotropic temperature factor increases.

Figure 9c shows the neutron diffraction pattern of the specimen irradiated at 280 °C and it is fit with one-layer model. The refinement results are listed in table 4 too. Compared to the other two samples, this sample is totally turbostraticly disordered since there is no three dimensional peaks any more. The small fraction of low strain, in-plane lattice constant, and the lateral size indicate that there is large distortion in plane. The large probability of random shift layers, interplanar spacing and its fluctuation shows that there are many of interstitial atoms in the space between two adjacent planes. The crystallite size is much smaller than the other two samples. All of these parameters indicated that the fast neutron irradiation damage is large in this sample.

Table 4. The results of the unirradiated and irradiated graphite samples. P is probability of random stacking of two-layer package (two-layer model) or layer (one-layer model); P_t is the probability of 3R stacking; d is the average distance of the two nearest layers; $(<\delta^2>)^{1/2}$ is the d-spacing fluctuation of the two nearest two-layer packages (two-layer model) or layers (one-layer model); M is the number of two-layer packages (two-layer model) or layers (one-layer model); La is the lateral dimension; a is lattice parameter; P_0 is the parameter of preferred orientation; g is the fraction of low strain; ζ is the in-plane strain parameter; and B is the Debye-Waller factor. The number with * is fixed in refinement.

sample	SGL-NBG-10-S2 (not irradiated)	GEN IVl03-124-l69 ($4.7x10^{25}$ n/m^2, 700 °C)	GEN IV L03-115-L25 ($4.9x10^{25}$ n/m^2, 280 °C)
d_{002} (Å)	3.3487(1)	3.3509(2)	3.462(1)
a (Å)	2.4539	2.4511	2.4069(9)
P	0.4164(20)	0.6368(51)	1.0*
P_t	0.1567(18)	0.1052(44)	
1-P-P_t	0.4269	0.2580	
$(<\delta^2>)^{1/2}$ (Å)	0.0102(2)	0.0204(6)	0.31(2)
g			0.40(2)
ζ			0.0661(8)
M	17.44(5)	15.1(1)	8.3(3)
La (Å)	238.17(3)	237.95(6)	42.454(8)
P_0	0.035(5)	0.11(1)	0*
B (Å^2)	0.93(2)	1.33(4)	1.28(5)
χ^2	15.5	8.7	1.8

Positron Annihilation Measurements

Graphite is well known to be a highly porous material. To assess the structure of the porosity measurements using positron annihilation lifetime spectrometry (PALS) were performed on the above listed graphite samples. A Na-22 based digital bulk PALS system has been used for this purpose. The pictures below show the system including the gamma-ray detectors (BaF_2 and $LaBr_3$) and data acquisition electronics. As a starting point, base-line measurements were also performed using Mercury

Intrusion Porosimetry (MIP), which gives pore size distributions for open pores. Nonetheless, this information is useful to establish base-line comparisons between PALS and MIP. In addition, PALS is expected to be focused on nanometer size pores, which are typical of sizes produced during the radiation damage stage and the subsequent stages of damage evolution. Figure 10 below shows MIP information for a "typical" reactor grade graphite sample.

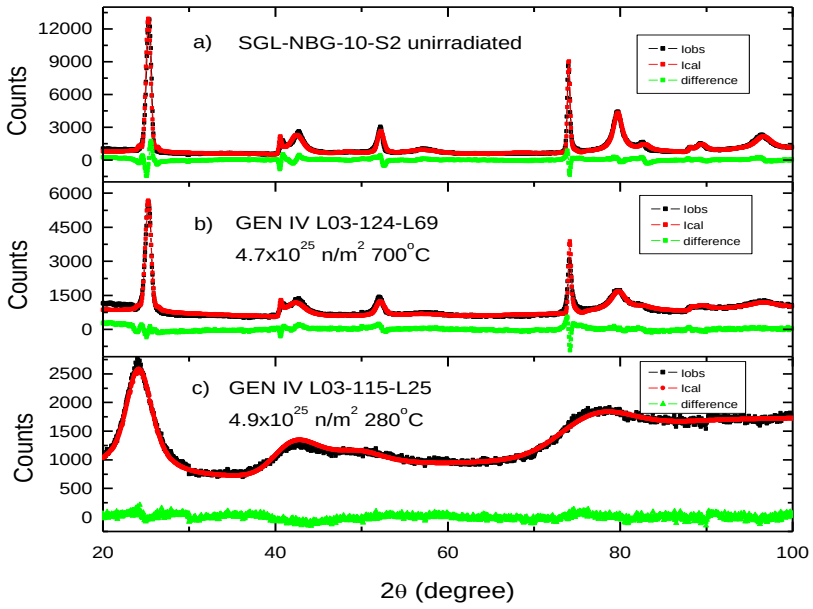

Fig. 9. The neutron diffraction patterns of the unirradiated and irradiated reactor grade graphite samples. The observed and calculated intensities are marked with black squares and red spot respectively. The green line gives the difference at each step.

Figure 11 below shows representative PALS data for unirradiated and irradiated (see Fig. 7) graphite samples.

The interpretation of the PALS measurements confirmed that upon irradiation the concentration of nano-vacancy clusters increases upon irradiation. By comparison to ab initio atomistic simulations, the clusters were estimated to be composed of the aggregation of 4 to 9 vacancies.

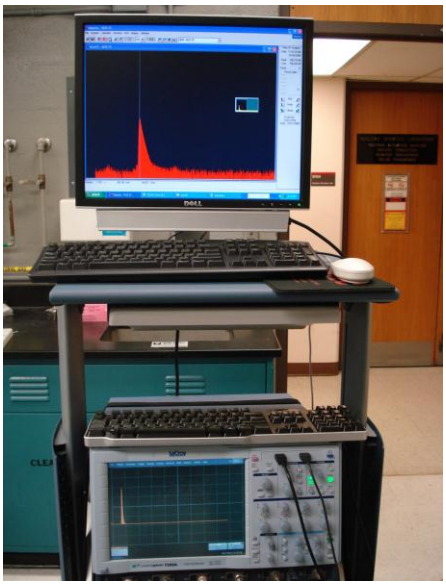

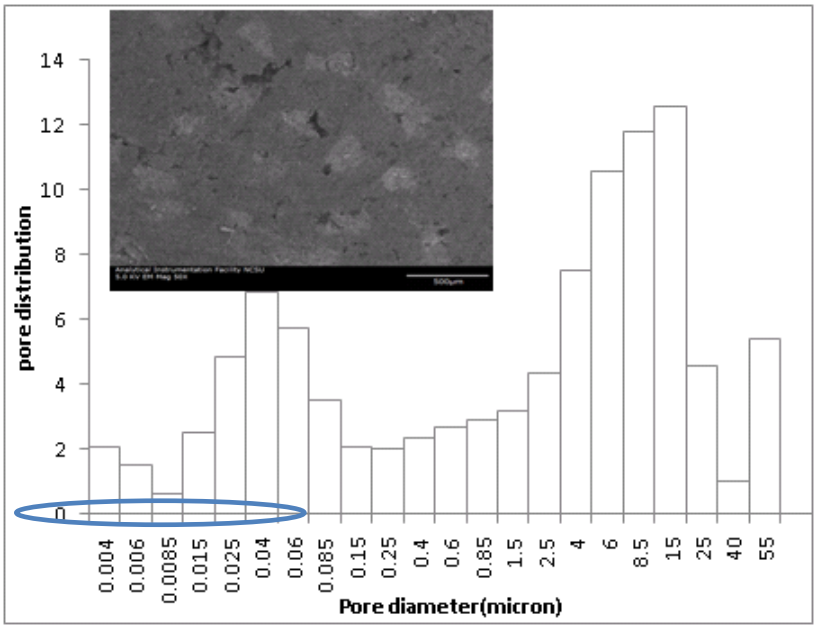

Fig. 10. The pore size distribution for a reactor grade graphite sample obtained using MIP. The circled region shows the pore size range that is expected to be sensitive to PALS. In this nm range, PALS is expected to be a more sensitive technique as it is capable of accessing open and closed pores, which would be important to comparing unirrdiated and irradiated graphite. The figure inset shows an SEM of the sample which clearly demonstrates the structure of reactor grade graphite.

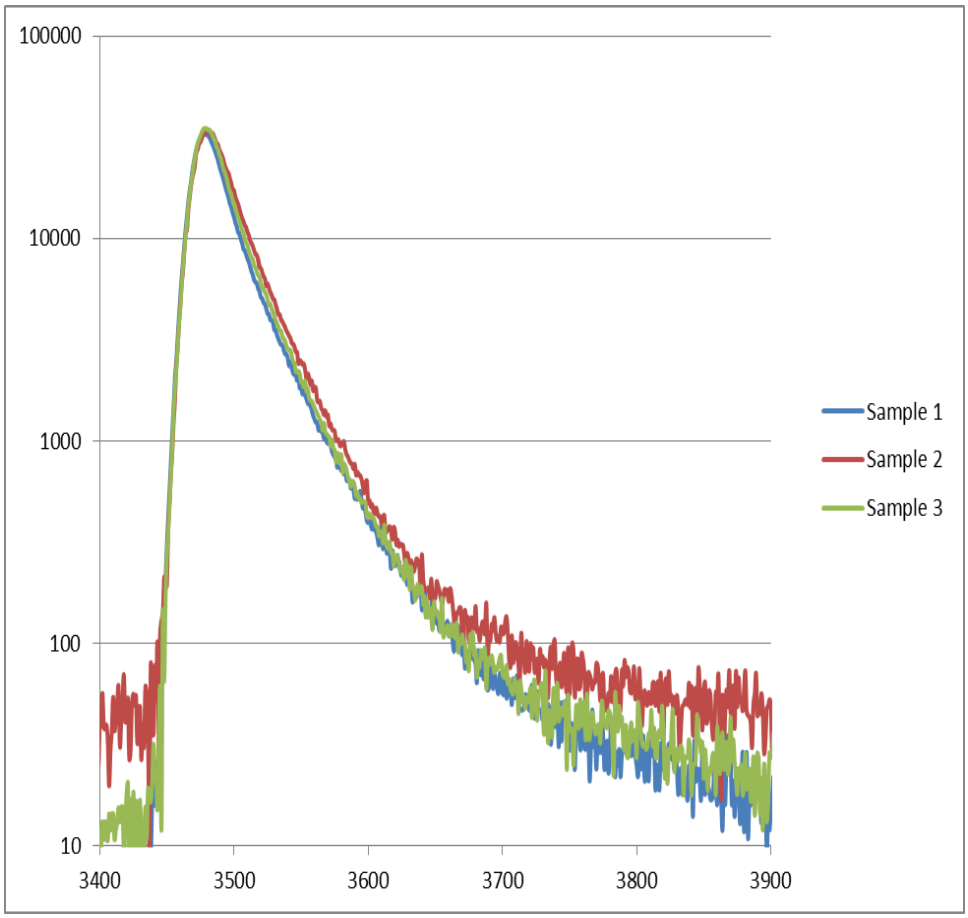

Fig. 11. Representative PALS spectra of unirradiated (sample 1) and irradiated graphite samples (sample 2 at 280°C and sample 3 at 700°C).

Neutron Scattering Dynamic Measurements

During this project time was obtained to perform neutron scattering measurements at the SEQUOIA instrument that is located at the Spallation Neutron Source (SNS) of ORNL. SEQUOIA is a direct geometry time-of-flight chopper spectrometer with fine energy transfer (ω) and wave-vector (Q) resolution that is utilized in high-resolution inelastic neutron scattering studies of magnetic excitations and fluctuations and lattice vibrations.

In this work, the measurements were performed on the irradiated graphite samples that were irradiated at 280°C (see Fig. 7). Figure 12 below

shows the measured scattering law for irradiated graphite as it compares to calculated data. The measurements show clearly that neutron irradiation results in a smoothing of the structure at the higher β range, which is consistent with the observations of MD simulations as it pertains to the smoothing of the density of states at higher energies.

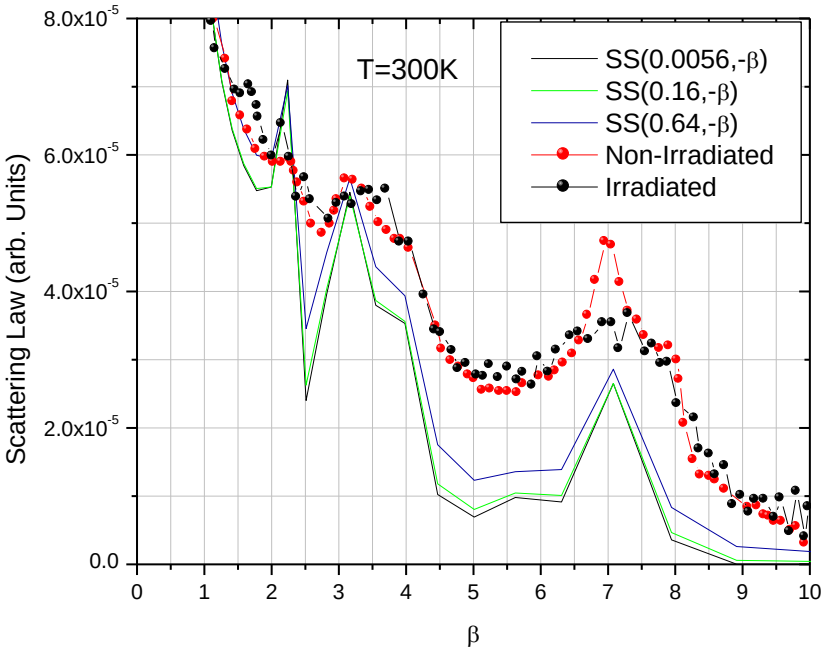

Fig. 12. The scattering law of graphite as measured at the SEQUOIA instrument at SNS. The irradiated data shows a diminishment of the peak around β=7, which is consistent with MD simulations.

5. Summary

This project utilized classical molecular dynamics simulations to model graphite and calculate the thermal neutron scattering cross sections. The predictions of the MD were combined with and compared to various types of measurements that aimed at exploring the structure and dynamics of graphite. Namely, elastic scattering powder neutron diffraction measurements were used to study the graphite atomic structure, positron annihilation measurements were used to investigate the porosity structure, and inelastic neutron scattering measurements were used to explore graphite dynamics.

As a result, a holistic simulation methodology was developed that is capable of producing accurate predictions of the thermal neutron scattering cross sections of both unirradiated and irradiated graphite. The observations of the simulations were found to be in agreement with the measurements observations.

The MD models were also used to estimate the stored energy in graphite as a result of irradiations. The results indicated good agreement with the estimated stored energy as reported in the literature for heavily irradiated graphite.

The produced thermal neutron scattering data has been formatted as libraries that can be used in VHTR design calculations.

Related Publications

Several publications related to this project were produced:

1) Hehr, B.D., Hawari, A.I., Gillette, V.H., “Generation of Graphite Thermal Neutron Scattering Libraries Using Classical Molecular Dynamics,” Transactions of the American Nuclear Society, v. 102, 2010.

2) DiJulio, D.D., Hawari, A.I., “Examination of reactor grade graphite using neutron powder diffraction,” Journal of Nuclear Materials, v. 392, n. 2, p 225-9, 2009.

3) Hehr B.D., Hawari A.I., "Evaluating the Graphite Thermal Neutron Scattering Law Using Molecular Dynamic Correlation Functions", International Conference on Advances in Mathematics, Computational Methods, and Reactor Physics, Saratoga Springs, New York, 2009.

4) Hehr, B.D., Hawari, A.I., “Molecular dynamics calculations of the thermal neutron scattering cross sections of graphite,” Transactions of the American Nuclear Society, v. 98, 2008.

5) DiJulio, D.D., Hawari, A.I., “Neutron scattering experiments in reactor grade graphite,” Transactions of the American Nuclear Society, v. 98, 2008.

Milestone Status:

Phase 1:

ID Number	Task / Milestone Description	Planned Completion	Actual Completion	Comments
(a)	Begin performing simulations of damage cascade initiation in graphite using neutron spectra supplied by INL	06/30/2008	06/30/2008	
(b)	Use the developed damage structure as input to ab initio calculations (using the VASP and PHONON codes) to establish the characteristic dispersion relations and the phonon density of states.	06/30/2008	06/30/2008	Used classical MD techniques as they proved more tractable for such analysis.
(c)	Use the calculated phonon information as input to the LEAPR module of the NJOY code to calculate the scattering law under the incoherent approximation and derive the scattering cross sections.	06/30/2008	06/30/2008	
(d)	Using the results of the atomistic simulations, derive the Wigner (stored) energy	06/30/2008	06/30/2008	
(e)	Begin experiments at ORNL to search for the high-temperature Wigner effect	06/30/2008	06/30/2008	Experiments were performed by ORNL.
(f)	Initiate experimental arrangements at NIST to perform density of states measurements	06/30/2008	06/30/2008	
(g)	Begin structure measurements using the NCSU neutron diffractometer facility	06/30/2008	06/30/2008	
(h)	Establish and begin executing VHTR benchmarks at INL to test the generated cross section libraries	06/30/2008	06/30/2008	

Phase 2:

ID Number	Task / Milestone Description	Planned Completion	Actual Completion	Comments
(a)	Continue the generation of the dose and temperature dependent thermal neutron scattering cross sections for graphite. Use NCSU developed methods to include the coherent inelastic scattering component in the calculation of the cross sections	06/30/2009	06/30/2009	
(b)	Establish the systematic behavior (obtained from cascade evolution simulations) of the Wigner (stored) energy for irradiated graphite at various irradiation temperatures	06/30/2009	06/30/2009	
(c)	Begin the measurements at SNS/NIST to obtain irradiated graphite density of states	06/30/2009	On-going	
(d)	Continue structure measurements using the NCSU neutron diffractometer facility	06/30/2009	On-going	
(e)	Continue experiments at ORNL to study the high-temperature Wigner energy phenomenon	06/30/2009	06/30/2009	
(f)	Perform reactor physics and engineering calculations at INL to study the effect of radiation damage (including any high temperature Wigner effect) on the neutronic, operational, and safety characteristics of VHTRs	06/30/2009	06/30/2009	

Phase 3:

ID Number	Task / Milestone Description	Planned Completion	Actual Completion	Comments
(a)	Finalize the generation of the dose and temperature dependent cross section libraries.	05/31/2011	05/31/2011	
(b)	Compare and interpret the experimental and computational findings on the density of state measurements	05/31/2011	05/31/2011	
(c)	Compare and interpret the experimental and computational findings on Wigner energy.	05/31/2011	05/31/2011	Computational and experimental data generated.
(d)	Finalize the reactor design calculations at INL and incorporate the consequences of using the irradiated graphite data into the operational and safety envelopes of VHTRs	05/31/2011	05/31/2011	Computational data generated and formatted for executing benchmarks.

Budget Data (08/30/2011):

NC State University			Approved Spending Plan			Actual Spent to Date		
Phase / Budget Period			DOE Amount	Cost Share	Total	DOE Amount	Cost Share	Total
	From	To						
Phase 1	06/01/07	05/31/08	$181,224	$46,138	$227,362	$74,349	$23,068	$97,417
Phase 2	06/01/08	05/31/09	$189,456	$46,620	$236,076	$78,172	$13,534	$91,706
Phase 3	06/01/09	05/31/11	197,999$	$50,776	248,775$	$416,158	$106,932	$523,090
		Totals	$568,679	$143,534	$712,213	$568,679	$143,534	$712,213